UC Santa Barbara
UC Santa Barbara Previously Published Works

Title

Probing Water Density and Dynamics in the Chaperonin GroEL Cavity

Permalink

https://escholarship.org/uc/item/9br2d0fp

Journal

Journal of the American Chemical Society, 136(26)

ISSN

0002-7863

Authors

Franck, John M
Sokolovski, Miri
Kessler, Naama
et al.

Publication Date

2014-07-02

DOI

10.1021/ja503501x

Peer reviewed

# Probing Water Density and Dynamics in the Chaperonin GroEL Cavity

John M. Franck,[†] Miri Sokolovski,[§] Naama Kessler,[§] Erez Matalon,[‡] Michal Gordon-Grossman,[‡] Song-i Han,*[,†] Daniella Goldfarb,*[,‡] and Amnon Horovitz*[,§]

[†]Department of Chemistry and Biochemistry, University of California Santa Barbara, California 93106, United States
[§]Departments of Structural Biology and [‡]Chemical Physics, Weizmann Institute of Science, Rehovot 76100, Israel

S Supporting Information

ABSTRACT: ATP-dependent binding of the chaperonin GroEL to its cofactor GroES forms a cavity in which encapsulated substrate proteins can fold in isolation from bulk solution. It has been suggested that folding in the cavity may differ from that in bulk solution owing to steric confinement, interactions with the cavity walls, and differences between the properties of cavity-confined and bulk water. However, experimental data regarding the cavity-confined water are lacking. Here, we report measurements of water density and diffusion dynamics in the vicinity of a spin label attached to a cysteine in the Tyr71 → Cys GroES mutant obtained using two magnetic resonance techniques: electron-spin echo envelope modulation and Overhauser dynamic nuclear polarization. Residue 71 in GroES is fully exposed to bulk water in free GroES and to confined water within the cavity of the GroEL−GroES complex. Our data show that water density and translational dynamics in the vicinity of the label do not change upon complex formation, thus indicating that bulk water-exposed and cavity-confined GroES surface water share similar properties. Interestingly, the diffusion dynamics of water near the GroES surface are found to be unusually fast relative to other protein surfaces studied. The implications of these findings for chaperonin-assisted folding mechanisms are discussed.
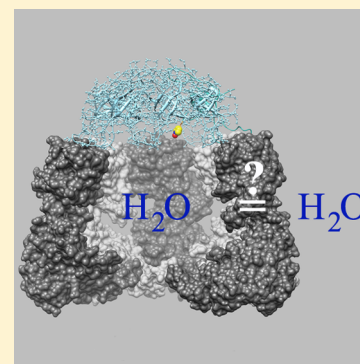
INTRODUCTION

The *Escherichia coli* GroE chaperonin system facilitates protein folding *in vivo* and *in vitro* in an ATP-dependent manner (for reviews see, for example, refs 1−3). It comprises GroEL, an oligomer of 14 identical subunits that form two heptameric rings, stacked back-to-back, with a cavity at each end[4] in which protein folding can take place in a protective environment, and its helper-protein GroES, which is a homoheptameric single ring. The GroE system is essential for the folding of only a small subset of *E. coli* proteins (<100) but what distinguishes GroE clients from all other *E. coli* proteins remains unclear.[5] Obligate substrates or other non-native proteins can become encapsulated in the GroEL cavity when GroES binds to the apical domains[6] of a substrate- and ATP-occupied GroEL ring. The substrates are then discharged into bulk solution, either folded or not, following GroES dissociation that is triggered by ATP hydrolysis in the GroES-bound *cis* GroEL ring and ATP binding to the opposite *trans* GroEL ring (see refs 2 and 7 for detailed schemes of current models of the GroE reaction cycle). The reaction cycle of GroEL is governed by the cooperative binding of ATP that is positive within rings and negative between rings.[2] The intraring positive allostery facilitates cycling of the GroEL rings between protein substrate acceptor and release states. Inter-ring negative allostery ensures that the two rings can operate out-of-phase with respect to each other and that ATP binding to one ring triggers GroES release from the opposite ring.[1−3] However, the role of the inter-ring allostery is less clear when the symmetric "football-shaped"

GroEL−GroES₂ complex (and not the asymmetric GroEL−GroES complex) is the active species of this nanomachine.[7]

Despite more than two decades of intensive research, it remains unclear and controversial whether the cavity of the GroEL−GroES complex is only a "passive cage" in which aggregation is prevented but the folding pathway is unchanged[8] or a chamber that has evolved to optimize the folding process itself.[9,10] Factors that could influence the folding reaction inside the GroEL cavity are steric confinement,[9,10] the chemical nature of the cavity walls[9,10] and the properties of the cavity-confined water, which may, in fact, be intimately linked to the steric and/or chemical effects of the confinement imposed by the GroEL interior surface.[11] The extent of steric confinement and the chemical nature of the cavity walls are known from the crystal structure of the GroEL−GroES complex,[6] but there is no available experimental data regarding the properties of the cavity water. Specifically, insight into the diffusion dynamics of water within the GroEL cavity can offer critical clues about the GroEL surface water attraction and may allow us to hypothesize about the stability and folding potential of proteins entering the GroEL cavity. If water is interacting favorably with the interior surface of the GroEL cavity, as would be reflected in strongly retarded, rigidified, surface water dynamics,[12] then a protein substrate that is encapsulated in the cavity will experience a strongly repulsive hydration barrier from the GroEL surface

and, thus, tend to fold in order to bury its hydrophobic residues.[11] By contrast, the hydrophobic nature of the cavity walls in GroEL's substrate acceptor state[4,6] may be reflected in nonretarded, fast diffusing, surface water dynamics that disfavor substrate folding. Equally interesting is the surface of the GroES lid: is it strongly or weakly hydrated and do the hydration level and dynamics change upon formation of the GroEL−GroES complex? The hydration properties of the GroEL cavity have been the focus of computational studies that indicated, for example, that GroEL's ability to assist folding scales with the affinity for water of the cavity's interior surface.[11] However, direct experimental measurements of properties of confined water in the GroEL cavity have not yet been reported. In this study, we present the first such experimental measurements for water near the surface of free GroES and the same surface when it faces the cavity of the GroEL−GroES complex.

The experiments described here combine site-directed spin labeling (SDSL) with two state-of-the-art magnetic resonance techniques: electron-spin echo envelope modulation (ESEEM) and Overhauser dynamic nuclear polarization−enhanced nuclear magnetic resonance (ODNP-NMR). A single site, Tyr71, in GroES was replaced by site-directed mutagenesis with a cysteine to which a nitroxide spin label, N-(1-oxyl-2,2,5,5-tetramethyl pyrrolidinyl)-maleimide, was attached. This position was chosen since it is fully exposed to bulk water in unbound GroES and, upon GroEL−GroES complex formation, faces the confined water inside the chaperonin cavity (Figure 1A,B).

Importantly, the spin label at this position is sufficiently far-removed from residues in the cavity wall, with the closest residue being Asn299, whose C_β side-chain atom is about 17 Å away from the nitroxide oxygen. The single-ring (SR1) version of GroEL with the mutation Asp398 → Ala that slows ATP hydrolysis considerably[13] was studied here instead of wild-type GroEL in order to minimize dissociation of the labeled GroES from GroEL. The cavity properties and intraring allostery[14,15] of SR1 are similar to those of wild-type GroEL.

ESEEM and ODNP-NMR spectroscopy at X-band (∼10 GHz) frequencies and a magnetic field of 0.35 T were employed to probe the properties of local water within the chaperonin cavity. In order to probe the amount of water in the vicinity of the spin label that protrudes into the cavity of the GroES−GroEL complex and can sense its upper region, the well-established ESEEM technique was employed for measuring hyperfine interactions between the electron spin of the label and nearby nuclear spins.[16] When the hyperfine interaction is very weak, its isotropic part is zero and the anisotropic part can be described by the point dipole interaction between the electron spin and the nuclear spin, whose strength is inversely proportional to the cube of their distance, r. In such cases, this interaction is manifested as modulations in the electron spin echo decay that oscillate at a frequency equal to the Larmor frequencies of the coupled nuclei, and the number of weakly coupled magnetic nuclei and their average distances from the electron spin are reflected in the modulation depth. By combining ESEEM of ^2H nuclei in D_2O solutions with spin labeling, it is possible to probe the number of D_2O molecules in the vicinity of the spin-labeled residue Cys71 (up to about 8 Å) without interferences from the protein protons. This method has been successfully used to derive the water penetration depth in membranes[17,18] and water exposure of protein residues.[19,20]
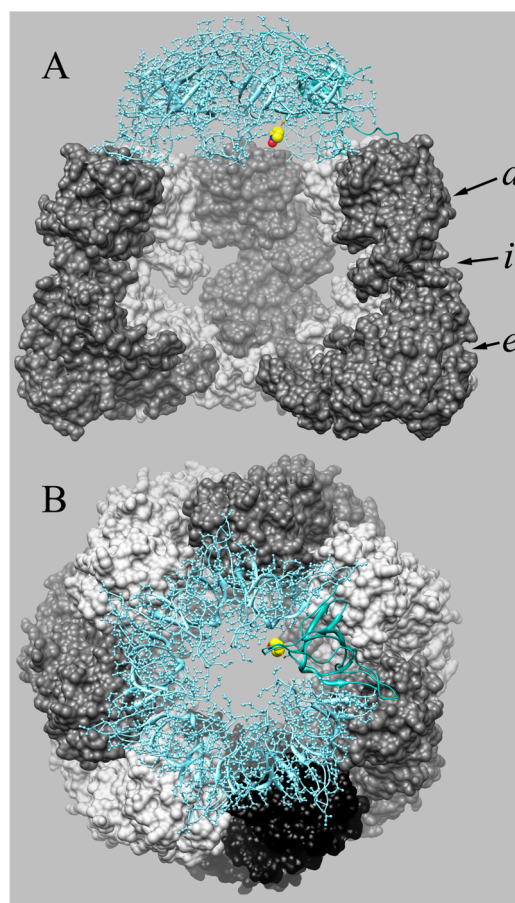

Figure 1. (A) Side and (B) top views of single-ring GroEL in complex with spin-labeled GroES. GroEL and GroES in the crystal structure of the GroEL−GroES complex (PDB code: 1AON)[6] are represented by space-filling (in gray) and ball-and-stick (in magenta) models, respectively. The labeled GroES subunit is shown in a darker magenta. The sulfur, carbon, nitrogen, and oxygen atoms of the spin label are shown in orange, yellow, blue, and red, respectively. In panel A, the apical, intermediate and equatorial domains are designated by a, i, and e, respectively, and two subunits of GroEL were removed in order to reveal the cavity. In the single-ring GroEL−GroES complex, the spin-labels are exposed to confined water in the cavity and are not close to any residues of GroEL. The figure was generated using the Chimera software.[51]

ESEEM measurements are usually carried out in frozen solutions and cannot probe the dynamic properties of protein surface water. To get information regarding dynamics under solution conditions at room temperature, we applied ODNP-NMR relaxometry[21,22] to probe the diffusion dynamics of water near the spin-labeled Cys71. ODNP selectively amplifies the ^1H NMR signal of the local hydration water around a specific spin label (within 5−10 Å) of a protein site by transferring polarization from the electron spin to the nearby moving water molecules using the same anisotropic hyperfine interaction mentioned above (alternatively termed the electron-nuclear dipole−dipole interaction). ODNP relies on the enhancement of the ^1H NMR signal of water at 0.35 T and ∼15 MHz that is achieved by saturating the electron spin resonance (ESR) transitions at ∼10 GHz. Since only the ^1H of water molecules that move fast (relative to ∼10 GHz) experience electron-^1H spin flip-flops that give rise to ^1H NMR signal enhancement, ODNP can be exploited to quantify local water diffusivity near the nitroxide spin label. The motion of hydration water is

characterized by a translational diffusion correlation time (τ_c), which represents the time needed for water to diffuse near the spin label within a distance b (typically 5–10 Å, as determined by the electron-^{1}H dipolar coupling field) and is inversely proportional to the local diffusion coefficient (D), i.e., with $\tau_c \propto b^2/D$. Crucially, ODNP, when combined with ^{1}H NMR relaxation time measurements, can separate contributions of freely diffusively translating hydration water (k_σ, picosecond time scale) from motional fluctuations that occur on a slower time scale (k_{low}, nanosecond time scale).[22] Weak protein surface water attraction will be reflected in small τ_c and large D and large k_σ values. Strong protein surface water attraction will present the opposite trend of large τ_c and small D and small k_σ values. In addition, there can be contributions from strongly bound water on protein surfaces with lifetimes exceeding ~1 ns, whose presence would be reflected in a large k_{low} value that increases as the rotational tumbling of the protein is slowed, for example, upon immobilization or immersion in a viscous solvent. Using this approach, the hydration dynamics landscape around lipid membranes[23] and proteins[24,25] has been mapped out recently with site-specificity.

It should be noted that protein site-specific correlation times for hydration dynamics have also been measured using ultrafast laser methods that monitor the relaxation of water around an excited tryptophan electric dipole by probing time-resolved Stokes shifts.[26−29] In these studies, all the modes of electric dipolar rearrangements from fs to ps can be captured. Time constants of several ps have generally been assigned in these studies to reorientation of water molecules and slower time constants of tens of ps to slow/bound water or collective translational motion. Time scales of hundreds of ps have also been reported for specific protein sites. By contrast, values of τ_c of hundreds of ps determined using ODNP reflect, like in previous NMR relaxometry studies,[30,31] only the translational diffusive motion of water in equilibrium. Time scales derived from different physical measurements are, therefore, best compared in terms of a relative change (e.g., retardation factor)[22] to assess "slow" and "fast" water dynamics on or near a biological surface of interest.

Here, we report on measurements, using both the ESEEM and ODNP techniques, that indicate that the formation of the GroES−GroEL complex does not induce significant changes in the local water density, level of hydration, dynamics of surface water, or the dynamics of the spin label itself compared to those of free GroES. Interestingly, we find that the water dynamics at the GroES surface are minimally retarded relative to bulk water, unlike the significantly slowed water dynamics observed in cases of hydrophilic lipid membrane surfaces[32] or representative protein surfaces.[12] This implies that the GroES surface is not attracting water significantly and that the GroES surface-water vs bulk water−water interaction is balanced, so that the interaction of other biomolecular constituents (e.g., protein substrates) with the GroES surface is relatively unhindered.

■ MATERIALS AND METHODS

Molecular Biology. The gene coding for GroES fused to a His$_6$-tag at its C-terminus and containing the Tyr71 → Cys mutation was generated using the plasmid pOA[33] and the Quick-Change site-directed mutagenesis kit (Stratagene, La Jolla, CA). The His$_6$-tag was introduced in two steps using the forward (and corresponding back) primers: His-tag 1,5′-CAAA GGAGAGTTATCAATGCACCATCAC-CATCACCCATTTGATTCGTCCATTGCATGATCG-3′; His-tag 2,5′-GCACCATCACCATCACCATAATATTCGTCCATTGCAT-GATCG-3′. The Tyr71 → Cys mutation was introduced using the

forward primer: 5′-CGTTATTTTCAACGATGGCTGCGGTGT-GAAATCTGAGAAGATCG -3′ and the corresponding back primer. DNA sequencing of the entire GroES gene was carried out to verify that the desired construct was obtained.

Protein Purification. GroES was purified by growing E. coli TG1 cells bearing the plasmid described above overnight at 37 °C in 2xTY medium containing 50 μg/mL ampicillin. The overnight culture was diluted 1:100 in 2xTY medium containing 50 μg/mL ampicillin, grown overnight at 37 °C and harvested. The pellet was resuspended in 50 mM Tris-HCl buffer (pH 7.5) containing 10% (w/v) sucrose, centrifuged, and stored at −80 °C until further use. It was then resuspended in 50 mM Tris-HCl buffer (pH 7.5) containing 0.5 M NaCl, 10 mM β-mercaptoethanol, 10 mM imidazole (buffer A), and 1 mM phenylmethanesulphonylfluoride. The cells were disrupted by sonication and the lysate was clarified by centrifugation at 20,000 rpm for 30 min at 4 °C. The supernatant was loaded on a 5 mL HisTrap HP column (Amersham Pharmacia, Uppsala, Sweden), and GroES was eluted using a 10−500 mM imidazole gradient in buffer A. Fractions were analyzed by SDS-PAGE and those containing GroES were combined and concentrated using a Vivaspin device (Sartorius, Goettingen, Germany) with a 10 kDa cutoff filter. The concentrated protein was transferred into 50 mM Tris-HCl buffer (pH 7.5) containing 10 mM KCl and 10 mM MgCl$_2$ (G10K buffer) using a PD-10 desalting column (GE Healthcare, Uppsala, Sweden) and then concentrated again. Aliquots of protein were snap frozen in liquid nitrogen and stored at −80 °C.

Purification of SR1, a single-ring version of GroEL, with the Asp398 → Ala mutation was carried out as described previously.[34]

Spin Labeling of GroES. A 50-fold molar excess of the 3-maleimido-2,2,5,5-tetramethyl-1-pyrrolidinyloxy (3-maleimido-proxyl) spin probe (Sigma) was added to the GroES Tyr71 → Cys mutant in D$_2$O G10K buffer and the suspension was then shaken for 16 h at 37 °C. Under these conditions, complete labeling is assumed to occur. Excess spin label was separated from the labeled GroES by using MicroSpin G-25 buffer exchange columns (GE Healthcare, Uppsala, Sweden). The labeled GroES was divided into aliquots, snap-frozen in liquid nitrogen and stored at −80 °C. ESEEM and ODNP experiments were not carried out using the more standard S-(2,2,5,5-tetramethyl-2,5-dihydro-1H-pyrrol-3-yl)methylmethanesulfonothioate (MTSL) label since GroES in complex with GroEL loses this label over time for reasons that are not clear.

Sample Preparations. The ESR and ESEEM experiments were carried out using an SR1−GroES complex that was prepared by incubating 1 mM ATP with 12 μM SR1 for 30 s and then adding labeled GroES (all in D$_2$O G10K buffer) and incubating for an additional 5 min. The molar ratio between SR1 and labeled GroES was 1.5:1, respectively, in order to ensure that all the labeled GroES is GroEL bound. This was verified routinely using gel-filtration chromatography. The ODNP experiments were carried out using 240 μM labeled or unlabeled GroES and a 1.5 molar excess of SR1 in G10K buffer containing 4 mM ATP and 21% (w/v) Ficoll 70 where indicated.

ESR and ESEEM Measurements. All CW X-band (9.5 GHz) measurements were performed at room temperature (22−25 °C) on a Bruker ELEXSYS E500 spectrometer, using round quartz capillaries (0.75 mm i.d. and 1 mm o.d.).

ESEEM experiments were carried out at 80 K on a Bruker ELEXSYS E580 spectrometer (9.5 GHz) using an ER4118X-MS-5 probe-head with a split ring resonator (5 mm sample access) on ~50−60 μL sample volumes. The ESEEM experiments were carried out using the three-pulse sequence $\pi/2$-τ-$\pi/2$-T-$\pi/2$-τ-echo, with a repetition time of 2.5 ms and a four-step phase cycling, in the presence of a magnetic field set to maximum echo intensity.[35] The $\pi/2$ pulse length was 16 ns. The τ-value was optimized to maximize the modulation depth of ^{2}H, i.e., $\tau = 1/(2\nu_D)$ while minimizing the modulation depth of ^{1}H, i.e. $\tau = 1/(\nu_H)$, yielding $\tau = 208$ ns, where $\nu_{H/D}$ is the ^{1}H or ^{2}H Larmor frequency, respectively. The time interval T was incremented in 20 ns steps starting at 60 ns for a total number of 250 points. The ESEEM modulation was isolated from the signal trace and its Fourier transform (FT-ESEEM) as follows: (1) phase
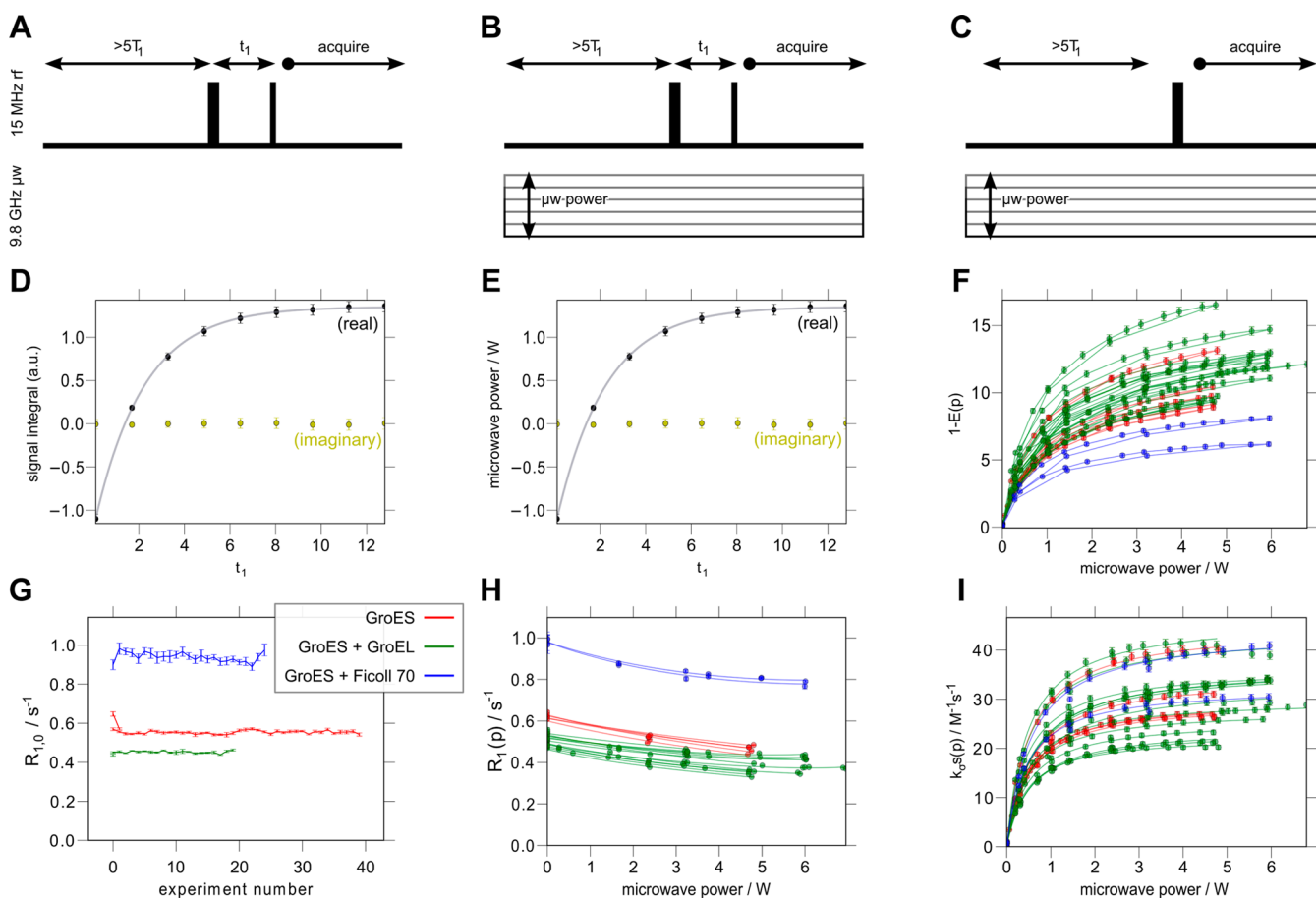
Figure 2. Outline of the complete procedure for ODNP data processing is shown for representative data. First, a variety of NMR measurements is carried out including an inversion recovery sequence acquired on a sample without spin label (A), a series of inversion recovery sequences acquired with spin label and different microwave powers (B), and a simple NMR spectrum acquired at different powers of ESR-resonant microwaves (C). The data corresponding to these pulse sequences are shown in panels D−F. The inversion−recovery curves (D, E) are fitted to determine the NMR relaxation rates $R_{1,0}$ (G) and $R_1(p)$ (H). The latter multiplies $1 − E(p)$ (F) to yield $k_\sigma s(p)$ (I), which are fitted to an asymptotic curve (shown as a solid line), allowing us to extrapolate it to full saturation of the ESR transition and determine $k_\sigma \approx k_\sigma s_{max}$. The multiple curves in panels F, H and I are for repeated experiments as indicated by the color code in panel G.

correction; (2) normalization; (3) division with a fifth-order polynomial obtained from fitting the echo decay during the time interval T; (4) subtraction of unity; and (5) apodization with a Hamming window, zero filling to 4096 points, FT and cross-term averaging.[36,37] The data are then displayed in magnitude mode. All experimental ESEEM traces were treated identically. We chose the intensity of the ^{2}H peak, $I(^2H)$, in the FT-ESEEM as a characteristic of the ^{2}H ESEEM pattern that reflects the modulation depth and, in turn, indicates the deuterium density around the spin label.[18,37−39]

ODNP Measurements and Data Analysis. Samples of ~3.1 μL in a 0.6 mm i.d. and 0.84 mm o.d. quartz capillary tube were analyzed by ODNP as described before,[22] using an NMR probe of a "pass-through" design built to fit inside a 3 mm i.d. and 6 mm o.d. quartz tube, which can be inserted into a high sensitivity (i.e., high Q) cavity (ER 4119HS-LC, Bruker Biospin). The samples were sealed inside the capillary with a protective layer of critoseal, followed by hot beeswax, and all ODNP measurements were performed at 20−24 °C. For these measurements, a microwave source and a homebuilt amplifier supplied up to 6 W at the ESR frequency (~9.8 GHz), and the field was set on resonance with the central ESR hyperfine transition, which was progressively saturated.

The presence of spin labels has two effects: (i) with or without microwave irradiation, the spin labels lead to a faster NMR relaxation rate, R_1 (Figure 2A,B); and (ii) in the presence of saturating microwaves, the ESR transition will cross-relax with the NMR transition of the ^{1}H nuclei of water (at a rate given by $k_\sigma C_{SL}$ as described below), thereby leading to an enhanced ^{1}H NMR signal

(Figure 2C). These two effects were quantified by carrying out NMR inversion recovery experiments (Figure 2A,B) and a series of basic NMR free induction decay (FID) experiments (Figure 2C) over a range of microwave powers. In both cases, the resulting NMR signals were Fourier transformed, baseline corrected, and integrated (pulse sequences in Figure 2A−C yield the respective data in Figure 2D−F). The integrated FT NMR signal from the FID experiments (Figure 2C) was normalized against the signal in the absence of microwave power to illustrate the increasingly larger enhancements (i.e. $E(p)$) obtained with increasing powers of saturating microwaves (Figure 2F). The inversion recovery data (Figure 2E) reflects the rate of recovery of the nuclear magnetization from the inverted state to equilibrium (i.e. $R_1(p)$). Finally, a control measurement is performed on a sample prepared without spin label. This consists of an inversion recovery experiment in the absence of microwave power (Figure 2A), which reflects the rate of recovery of magnetization to equilibrium in the absence of spin label, $R_{1,0}$ (note that here R_1 and $R_{1,0}$ refer to the inverses of the NMR spin−lattice relaxation times, i.e. $R_1 = T_1^{-1}$ and $R_{1,0} = T_{1,0}^{-1}$).

The data shown in Figure 2D−F were further processed to obtain the spin label-dependent relaxation rates, or relaxivities, that offer insight into the dynamics of the hydration water, as explained in more detail elsewhere.[22,40] The inversion recovery curves (e.g., Figure 2D, E) are fitted to obtain the NMR relaxation rates of samples without the spin label ($R_{1,0}$, Figure 2G) and with the spin label ($R_1(p = 0)$ from Figure 2H). The self-relaxation rate, $k_\rho C_{SL}$, is obtained by subtracting $R_{1,0}$ from $R_1(p = 0)$ (i.e., R_1 in the absence of microwave power). The

spin-label-driven proton self-relaxivity, k_ρ, is then obtained from the self-relaxation rate by normalizing against the spin label concentration (C_{SL}). The cross-relaxivity, k_σ, is determined from the data in Figure 2I, which are obtained by multiplying $1 - E(p)$, the amount of polarization transferred (Figure 2F), by the microwave power-dependent relaxation rate $R_1(p)$ (Figure 2H) and dividing by 659.3 (the ratio of the ESR to NMR resonance frequencies) and the concentration C_{SL}. These data are then fitted to an asymptotic curve to obtain a value for the cross relaxivity, $k_\sigma \approx k_\sigma s_{max}$ ($s_{max} \approx 1$, as shown previously)[41] where the value of $k_\sigma s(p)$ approaches complete saturation of the ESR transition at high microwave power.

The ratio of the relaxivities k_σ and k_ρ yields the coupling factor, ξ ($\xi = k_\sigma/k_\rho$). Given a specific field (and therefore resonance frequency), the force-free hard-sphere (FFHS) model for translational dynamics[42] provides a relationship that can be used to determine the translational correlation time, τ_c, from the measured value of ξ. In order to better understand the contribution of partially bound waters (which are not well modeled by FFHS) to the value of ξ, the contribution from the fast waters (i.e., k_σ) can also be subtracted from the self-relaxivities (k_ρ) as follows:

$$k_{low} = \frac{5}{3}k_\rho - \frac{7}{3}k_\sigma \qquad (1)$$

where k_{low} describes the slower time scale ($\sim$15 MHz) fluctuations of the dipolar interaction.[22] The value of ξ is related to the ratio between k_σ and k_{low}:

$$\xi = \frac{5k_\sigma/k_{low}}{3 + 7k_\sigma/k_{low}} \qquad (2)$$

where $0 \leq k_\sigma/k_{low} \leq 1$. Each measurement was repeated 2–4 times, and the standard deviations of the resulting values of ξ, k_σ, k_{low}, and τ_c are presented as errors (i.e., as value $\pm$ error). An analysis of the scatter in the data is shown in Figure S1.

■ RESULTS AND DISCUSSION

ESR Measurements. The X-band ESR spectrum of the spin labeled GroES (SL-GroES) in Figure 3 shows that the mobility
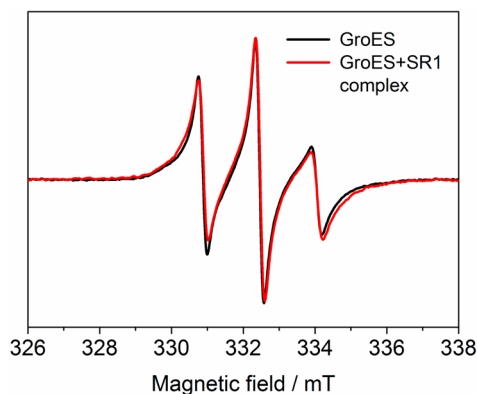
Figure 3. CW ESR spectra of the spin label attached to free GroES (black) and GroES in complex with SR1 (red) at room temperature in D_2O.

of the spin label at position 71 on the GroES surface (Figure 1) is restricted compared to a free spin probe and represents a single population, thus providing evidence that the spin label is attached to the protein. An estimate of 10^{-9} s for the rotational correlation time can be obtained from comparison to spectra simulated using Easyspin[43] and assuming isotropic motion. Notably, the ESR spectrum shows only very subtle broadening upon formation of the complex between SL-GroES and SR1, thus indicating that the mobility of the spin label hardly changes when it is encapsulated within the cavity.

The ESEEM results for SL-GroES and the SL-GroES–SR1 complex in D_2O solvent are presented in Figure 4. The peak at
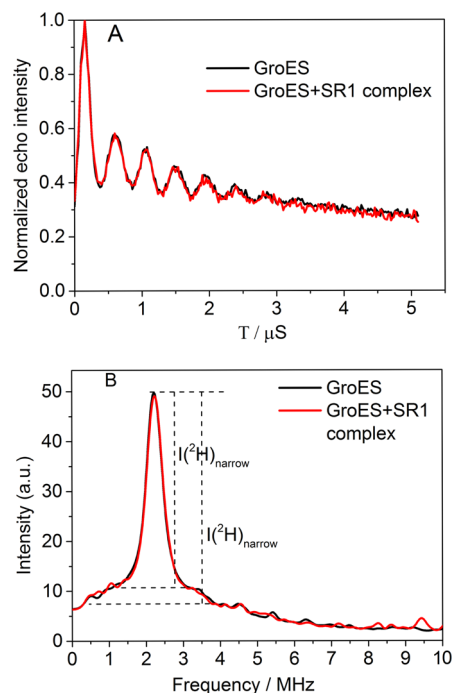
Figure 4. (A) Time domain traces of three-pulse ESEEM measured at 80 K and the corresponding (B) Fourier transforms for free (black) and SR1-bound spin-labeled GroES (red). For more details, see Materials and Methods.

the ^2H frequency with intensity $I(^2H)$ shows two components, where the broad resonance is due to water molecules H-bonded to the nitroxide moiety and the narrow component, $I(^2H)_{narrow}$, is due to more distant water molecules.[23] The time domain and FT-ESEEM traces for the SL-GroES and SL-GroES–SR1 complex samples are identical, thus indicating that there is no difference between the density of water near the spin label of free SL-GroES vs SL-GroES in complex with SR1. This implies that the number of water molecules and their distances from the spin label are the same in the two samples as reflected in the same $I(^2H) = 42$. For comparison, we also measured the $I(^2H)$ value for a free spin label dissolved in D_2O/glycerol-d_8 (7:3 v/v) and obtained $I(^2H) = 80$. Here, the addition of the glycerol was essential to prevent ice formation and aggregation of the spin probe upon freezing. A ratio of 0.5 is found between the $I(^2H)$ values for the SL-GroES by itself or in complex with SR1 and the free spin label. Assuming that glycerol-d_8 does not affect significantly the ^2H density in the sample (as glycerol was not present in the protein samples) and in the vicinity of the spin label, we can compare this value to the values of 0.54 and 0.18 that were obtained for the most exposed and buried MTSL-labeled sites, respectively, in the light harvesting protein complex IIb of photosystem II.[20] This is consistent with the spin label attached to GroES being exposed to bulk or the cavity water. Currently, there is no reliable theoretical model for extracting the actual water distribution in the vicinity of the spin probe, in the case of D_2O solutions, from fitting the experimental data. Consequently, the data are often fitted to a model based on assuming a spherical distribution of n ^2H nuclei around the spin label at an effective distance r.[44] We chose not to use such a model as it is not realistic and preferred, instead,

to interpret the experimental $I(^2H)$ values on a comparative basis.

ODNP Measurements. Representative R_1 and $R_{1\rho}$ data, as well as all the original ^1H NMR signal enhancement measurements as a function of microwave power, $E(p)$, are shown in Figure 2. These data were collected for three samples: free GroES in G10K buffer, GroES in complex with SR1, and GroES in a Ficoll 70 solution. From these data, $k_\sigma \approx k_\sigma s_{max}$ values were extracted, as well as the k_{low} values using eq 1, the coupling factor, ξ, and the translational diffusion correlation time, τ_c (see Table 1). The ratios between the k_σ, k_{low}, ξ, and τ_c

Table 1. Relativity, Coupling Factor, and Retardation Factor Values for GroES under Different Conditions[a]

	$k_\sigma/k_{\sigma,bulk}$	$k_{low}/k_{low,bulk}$	ξ/ξ_{bulk}	$\tau_c/\tau_{c,bulk}$
GroES−SR1 complex	0.36 ± 0.06	1.22 ± 0.24	0.40 ± 0.10	3.14 ± 0.72
GroES	0.34 ± 0.08	0.80 ± 0.35	0.55 ± 0.13	2.31 ± 0.55
GroES with Ficoll 70	0.40 ± 0.06	0.64 ± 0.20	0.73 ± 0.26	1.64 ± 0.75

[a]For derivation of the relativity values, see the text and Figure 2.

values for the spin label tethered to GroES and the free spin label in bulk solution are presented in Table 1 and Figure 5. It
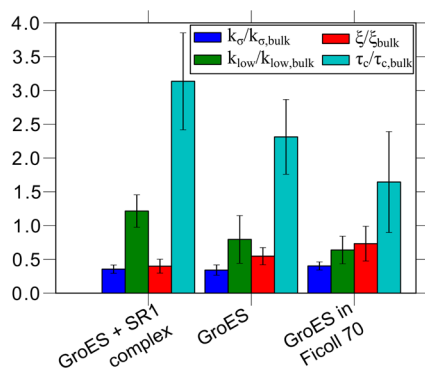

Figure 5. Bar plot of the values of the various ODNP measurements for free GroES in aqueous buffer, GroES in complex with SR1 and GroES in the presence of Ficoll 70. Shown are values of the cross-relaxivity, k_σ (blue), the slow-motion component of the self-relaxivity,[22] $k_{low} = 5/3k_\rho − 7/3k_\sigma$ (green), the coupling factor, ξ (red), and the translational correlation time, τ_c (cyan), which is determined by applying the FFHS model.[42] For simplicity, all quantities are normalized by the appropriate bulk values:[22] $k_{\sigma,bulk} = 95.4\ s^{-1}\ M^{-1}$, $k_{low,bulk} = 366\ s^{-1}\ M^{-1}$, $\xi_{bulk} = 0.27$, $k_\rho = 353\ s^{-1}\ M^{-1}$, and $\tau_{c,bulk} = 54$ ps.

can be seen that the values of these ratios are the same, within error, for SL-GroES and the SL-GroES−SR1 complex. Therefore, we will first discuss the meaning of the resulting average values and the fact that the value of k_σ remains completely unaltered—the key result presented here. The meaning of very small changes in $k_{low}/k_{low,bulk}$ that impact the value of ξ and τ_c (eq 2) will be discussed below. Interestingly, the value of $k_{low}/k_{low,bulk}$ that represents the contribution from slow time scale fluctuations is approximately 1, thereby indicating that it is likely that there is no bound water at the SL-GroES surface. This, by itself, is an interesting result as it is typical to find some contribution from bound water near protein surfaces, unlike at the surfaces of lipid membranes that

are known to have minimal or no contribution from bound water.[31] All the $k_\sigma/k_{\sigma,bulk}$ values are 0.4 ± 0.07 and, thus, reflect modest retardation and comparatively fast diffusive motion of the surface water hydrating the SL-GroES surface. These data clearly illustrate that the decrease in the ξ values relative to those of bulk water and the retardation of surface water dynamics as reflected in $\tau_c/\tau_{c,bulk}$ originate exclusively from changes in the contribution of fast moving, loosely bound, surface water, as reflected in k_σ. Moreover, the calculated value of 2−3 for the retardation factor, $\tau_c/\tau_{c,bulk}$, is exceptionally small compared to typical retardation factors of 5−10 or larger, as found for solvent-exposed protein surfaces of tau,[24] apomyoglobin[12] and other biomolecular or polymer surfaces[25,32] (Figure 6). All of these trends point to a highly lubricated, weakly hydrated, protein surface of SL-GroES. This weak hydration does not change, within error, upon complexation with SR1. To further test this conclusion, the measurements of water dynamics were repeated for SL-GroES in the presence of 21% (w/v) Ficoll 70, a known viscogen that does not interact
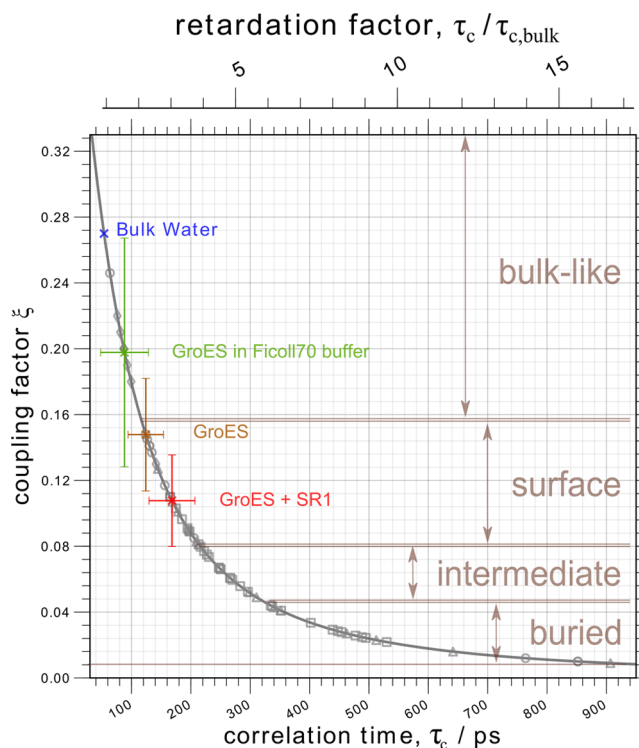

Figure 6. Plot of the coupling factor measurement, ξ, as a function of the modeled translational correlation time, τ_c. The data points for the ODNP measurements for free GroES, GroES in complex with SR1, and GroES in the presence of Ficoll 70 are in brown, red, and green, respectively. The FFHS model gives a fixed relationship, $\xi(\tau_c)$, for measurements at 0.35 T (corresponding to 15 MHz nuclear Larmor frequency) that is illustrated by the solid gray line. The gray symbols indicate previous ODNP measurements for a variety of proteins, small peptides, lipids, and DNA that are grouped (in brown text, to the right) according to the location of the spin label. As explained previously,[22] measurements in the zone designated "buried" were for labels attached within the core of a lipid bilayer, globular protein, or compact polymer system; in the zone designated "surface" for labels attached to the surfaces of proteins or other polymer; in the "intermediate" zone for labels attached near but not at the surface of, for example, a lipid bilayer; and in the "bulk" zone for small molecule nitroxides freely dispersed in water or certain highly charged polymers such as DNA.

with the protein surface but slows the overall protein tumbling time by increasing the bulk water viscosity by about 10-fold at 21% (w/v) concentration. Interestingly, the values for $k_{low}/k_{low,bulk}$, ξ/ξ_{bulk}, and $\tau_c/\tau_{c,bulk}$ are all, within error, unaltered, suggesting that there is no bound water population whose effect is masked due to fast protein tumbling in the absence of Ficoll 70. The contribution from fast moving water, as reflected in $k_\sigma/k_{\sigma,bulk}$, also remains unaltered and, in keeping with previous[40] observations on lipid surfaces, remains unaffected by the increase in the bulk solvent viscosity induced by Ficoll 70, thus confirming that this polymeric viscogen does not interact with the GroES surface.

Interestingly, the value of $k_{low}/k_{low,bulk}$ for the GroES/SR1 complex is found to be somewhat higher (and may exceed the error of measurement) than the corresponding values for GroES with or without Ficoll 70 (Figure 5). The increase in k_{low} leads to a slightly larger apparent retardation factor, thereby indicating slower hydration dynamics (see $\tau_c/\tau_{c,bulk}$ in Figure 5). To understand the subtle meaning of these changes, we recall that ODNP is sensitive to fluctuations in the spin–spin dipolar interaction between water and the spin label that is attached to the surface of GroES. The value of k_σ samples fluctuations with time constants of tens of picoseconds and faster (i.e., 10 GHz fluctuations). Fluctuations on this time scale are typically associated with water molecules freely diffusing past a spin label. Therefore, the change in k_{low} observed here does not reflect a change in the dynamics of freely translationally diffusing hydration water since such a change would also alter the value of k_σ. Rather, a selective increase in k_{low}, as observed here, indicates an increase in slower fluctuations, with time constants as low as 10 ns (i.e., 15 MHz fluctuations). Fluctuations on this time scale can arise either when, for example, water molecules near the spin label bind partially (for ns or tens of ns) to the surface of GroES as it tumbles in solution or when water molecules chemically exchange with labile protons on the protein surface near the spin label. Thus, it is possible that GroES/SR1 either might trap a limited number of partially bound water molecules or may engage the water in chemical exchange. Because the value of k_{low} is the same (within error) for GroES with or without Ficoll 70, this limited population of bound or exchanging waters would only be present in the chaperone complex and not on the surface of free GroES. However, most importantly, because the change in k_{low} is small (2-fold at most), we can assume that these changes indicate the presence of relatively few bound or exchanging water molecules. Even these small changes do not arise from changes in the freely translating water inside the nanocavity, as indicated by the consistent k_σ value.

We conclude that the SL-GroES surface is very weakly hydrated with highly mobile surface water, with no contribution of surface bound water, thus representing an unusual protein surface. There are indications that, upon formation of the SL-GroES−SR1 complex, a very select and small number of water molecules either bind partially to the cavity surface or engage in chemical exchange with it. However, it is clear that the majority of the water molecules continue to exhibit the same unusually high mobility and weak hydration even when confined inside the SL-GroES−SR1 cavity. This implies that the repulsive hydration barrier for a substrate to approach the GroES surface is very small and that the substrate experiences a bulk water-like environment, even upon confinement within the cavity of the SL-GroES−SR1 complex.

A previous computational study[11] suggested that the folding potential of proteins within the chaperonin cavity is enhanced owing to the hydrophilicity of the cavity inner surface, as measured by the density of surface water. When employing ODNP methods, a high hydrophilicity of a protein surface would be reflected in retarded surface water diffusivity because of the attraction of water to the protein surface. However, we observe rather unusually fast dynamics of water on the cavity-facing surface of GroES, both when it is free and when it is in complex with GroEL. ODNP-NMR does yield very slightly different results for the GroES/SR1 complex due to the presence of a small number of bound water molecules or labile protons on the inner surface of the cavity but does not yield results suggesting an overall slowing of the hydration water. The fast dynamics seen here have been seen for the surfaces of unstructured polymers[45,46] but have not been observed before in cases of proteins and lipid membranes (see Figure 6). These unexpectedly fast diffusion dynamics of the surface hydration water implies a low repulsive barrier for the substrate to approach (and leave) the GroES surface as well as a low folding potential for the substrate near the GroES surface. This suggestion that the GroES lid confers a low protein folding potential is in agreement with the finding[47] that replacing Tyr71 in GroES with charged residues enhances the GroEL-assisted folding of GFP. Our observation that the cavity-facing surface of the GroES lid has a low folding potential is also in agreement with the report that nonfolded substrate proteins can approach the lid and escape from the cage.[48]

■ CONCLUSIONS

In this study, the properties of the chaperonin cavity-confined water were studied using ESEEM and ODNP by attaching a spin label to a cysteine in the Tyr71 → Cys GroES mutant. This residue is fully exposed to bulk water in free GroES and can probe the confined water in the upper region of the cavity in the GroEL−GroES complex. Previous work has shown that replacement of Tyr71 in GroES with positively or negatively charged residues enhances GroE-assisted GFP folding,[47] thereby indicating that the position we labeled senses a region of the cavity that is of functional importance. Our main findings are that both the density and the dynamics of the water in the vicinity of the spin label are the same in free and SR1-bound GroES, and that the properties of the cavity-confined water are similar to those of bulk water. These findings are consistent with the claim that the folding process inside the GroEL cage is similar to that in bulk solution, i.e., that the GroEL cavity is a "passive" cage in which folding is not accelerated[8,49] and may even be slowed down.[50] It should be borne in mind, however, that the dynamics of the surface water closer to the bottom of the GroEL cavity may be vastly different (e.g., slower) than those of water at the top. Future studies need to be designed for probing the properties of water at the bottom of the cage and in the presence of nonfolded substrates.

■ ASSOCIATED CONTENT

ⓈSupporting Information

Figure showing correlation between the spin-label-induced relaxation rate and the ODNP cross-relaxation rate. This material is available free of charge via the Internet at http://pubs.acs.org.

AUTHOR INFORMATION

Corresponding Authors

songi@chem.ucsb.edu
Daniella.Goldfarb@weizmann.ac.il
Amnon.Horovitz@weizmann.ac.il

Notes

The authors declare no competing financial interest.

REFERENCES

(1) Thirumalai, D.; Lorimer, G. H. *Annu. Rev. Biophys. Biomol. Struct.* **2001**, *30*, 245−269.

(2) Horovitz, A.; Willison, K. R. *Curr. Opin. Struct. Biol.* **2005**, *15*, 646−651.

(3) Horwich, A. L.; Fenton, W. A. *Q. Rev. Biophys.* **2009**, *42*, 83−116.

(4) Braig, K.; Otwinowski, Z.; Hegde, R.; Boisvert, D. C.; Joachimiak, A.; Horwich, A. L.; Sigler, P. B. *Nature* **1994**, *371*, 578−586.

(5) Azia, A.; Unger, R.; Horovitz, A. *FEBS J.* **2012**, *279*, 543−550.

(6) Xu, Z.; Horwich, A. L.; Sigler, P. B. *Nature* **1997**, *388*, 741−750.

(7) Yang, D.; Ye, X.; Lorimer, G. H. *Proc. Natl. Acad. Sci. U.S.A.* **2013**, *110*, E4298−4305.

(8) Tyagi, N. K.; Fenton, W. A.; Deniz, A. A.; Horwich, A. L. *FEBS Lett.* **2011**, *585*, 1969−1972.

(9) Chakraborty, K.; Chatila, M.; Sinha, J.; Shi, Q.; Poschner, B. C.; Sikor, M.; Jiang, G.; Lamb, D. C.; Hartl, F. U.; Hayer-Hartl, M. *Cell* **2010**, *142*, 112−122.

(10) Tang, Y. C.; Chang, H. C.; Roeben, A.; Wischnewski, D.; Wischnewski, N.; Kerner, M. J.; Hartl, F. U.; Hayer-Hartl, M. *Cell* **2006**, *125*, 903−914.

(11) England, J. L.; Lucent, D.; Pande, V. S. *J. Am. Chem. Soc.* **2008**, *130*, 11838−11839.

(12) Armstrong, B. D.; Choi, J.; Lopez, C.; Wesener, D. A.; Hubbell, W.; Cavagnero, S.; Han. S. *J. Am. Chem. Soc.* **2011**, *133*, 5987−5995.

(13) Rye, H. S.; Burston, S. G.; Fenton, W. A.; Beechem, J. M.; Xu, Z.; Sigler, P. B.; Horwich, A. L. *Nature* **1997**, *388*, 792−798.

(14) Poso, D.; Clarke, A. R.; Burston, S. G. *J. Mol. Biol.* **2004**, *338*, 969−977.

(15) Amir, A.; Horovitz, A. *J. Mol. Biol.* **2004**, *338*, 979−988.

(16) Kevan, L. In *Time Domain Electron Spin Resonance*; Kevan, L., Schwartz, R. N., Eds.; John Wiley & Sons: New-York, 1979, 279−343.

(17) Erilov, D. A.; Bartucci, R.; Guzzi, R.; Shubin, A. A.; Maryasov, A. G.; Marsh, D.; Dzuba, S. A.; Sportelli, L. *J. Phys. Chem. B* **2005**, *109*, 12003−12013.

(18) Carmieli, R.; Papo, N.; Zimmermann, H.; Potapov, A.; Shai, Y.; Goldfarb, D. *Biophys. J.* **2006**, *90*, 492−505.

(19) Volkov, A.; Dockter, C.; Polyhach, Y.; Paulsen, H.; Jeschke, G. *J. Phys. Chem. Lett.* **2010**, *1*, 663−667.

(20) Volkov, A.; Dockter, C.; Bund, T.; Paulsen, H.; Jeschke, G. *Biophys. J.* **2009**, *96*, 1124−1141.

(21) Armstrong, B. D.; Han, S. *J. Am. Chem. Soc.* **2009**, *131*, 4641−4647.

(22) Franck, J. M.; Pavlova, A.; Scott, J. A.; Han, S. *Prog. Nucl. Magn. Reson. Spectrosc.* **2013**, *74*, 33−56.

(23) Kausik, R.; Han, S. *J. Am. Chem. Soc.* **2009**, *131*, 18254−18256.

(24) Pavlova, A.; McCarney, E. R.; Peterson, D. W.; Dahlquist, F. W.; Lew, J.; Han, S. *Phys. Chem. Chem. Phys.* **2009**, *11*, 6833−6839.

(25) Hussain, S.; Franck, J. M.; Han, S. *Angew. Chem., Int. Ed.* **2013**, *52*, 1953−1958.

(26) Zhong, D.; Pal, S. K.; Zewail, A. H. *Chem. Phys. Lett.* **2011**, *503*, 1−11.

(27) Pal, S. K.; Peon, J.; Zewail, A. H. *Proc. Natl. Acad. Sci. U.S.A.* **2002**, *99*, 15297−15302.

(28) Jurkiewicz, P.; Cwiklik, L.; Jungwirth, P.; Hof, M. *Biochimie* **2012**, *94*, 26−32.

(29) Zhang, L.; Yang, Y.; Kao, Y. T.; Wang, L.; Zhong, D. *J. Am. Chem. Soc.* **2009**, *131*, 10677−10691.

(30) Polnaszek, C. F.; Bryant, R. G. *J. Chem. Phys.* **1984**, *81*, 4038−4045.

(31) Hodges, M. W.; Cafiso, D. S.; Polnaszek, C. F.; Lester, C. C.; Bryant, R. G. *Biophys. J.* **1997**, *73*, 2575−2579.

(32) Cheng, C. Y.; Varkey, J.; Ambroso, M. R.; Langen, R.; Han, S. *Proc. Natl. Acad. Sci. U.S.A.* **2013**, *110*, 16838−16843.

(33) Horovitz, A.; Bochkareva, E. S.; Kovalenko, O.; Girshovich, A. S. *J. Mol. Biol.* **1993**, *231*, 58−64.

(34) Frank, G. A.; Kipnis, Y.; Smolensky, E.; Daube, S. S.; Horovitz, A.; Haran, G. *Bioconjugate Chem.* **2008**, *19*, 1339−1341.

(35) Fauth, J. M.; Schweiger, A.; Braunschweiler, L.; Forrer, J.; Ernst, R. R. *J. Magn. Reson.* **1986**, *66*, 74−85.

(36) Van Doorslaer, S.; Sierra, G. A.; Schweiger, A. *J. Magn. Reson.* **1999**, *136*, 152−158.

(37) Matalon, E.; Kaminker, I.; Zimmermann, H.; Eisenstein, M.; Shai, Y.; Goldfarb, D. *J. Phys. Chem. B* **2013**, *117*, 2280−2293.

(38) Baute, D.; Goldfarb, D. *J. Phys. Chem. C* **2007**, *111*, 10931−10940.

(39) Gordon-Grossman, M.; Gofman, Y.; Zimmermann, H.; Frydman, V.; Shai, Y.; Ben-Tal, N.; Goldfarb, D. *J. Phys. Chem. B* **2009**, *113*, 12687−12695.

(40) Franck, J. M.; Scott, J. A.; Han, S. *J. Am. Chem. Soc.* **2013**, *135*, 4175−4178.

(41) Armstrong, B. D.; Han, S. *J. Chem. Phys.* **2007**, *127*, 104508.

(42) Hwang, L. P.; Freed, J. H. *J. Chem. Phys.* **1975**, *63*, 4017−4025.

(43) Stoll, S.; Schweiger, A. *J. Magn. Reson.* **2006**, *178*, 42−55.

(44) Kevan, L.; Bowman, M. K.; Narayana, P. A.; Boeckman, R. K.; Yudanov, V. F.; Tsvetkov, D. *J. Chem. Phys.* **1975**, *63*, 409−416.

(45) Ortony, J. H.; Cheng, C. Y.; Franck, J. M.; Kausik, R; Pavlova, A.; Hunt, J.; Han, S. *New J. Phys.* **2011**, *13*, 015006.

(46) Kausik, R.; Srivastava, A.; Korevaar, P. A.; Stucky, G.; Waite, J. H.; Han, S. *Macromolecules* **2009**, *42*, 7404−7412.

(47) Wang, J. D.; Herman, C.; Tipton, K. A.; Gross, C. A.; Weissman, J. S. *Cell* **2002**, *111*, 1027−1039.

(48) Motojima, F.; Yoshida, M. *EMBO J.* **2010**, *29*, 4008−4019.

(49) Apetri, A. C.; Horwich, A. L. *Proc. Natl. Acad. Sci. U.S.A.* **2008**, *105*, 17351−17355.

(50) Hofmann, H.; Hillger, F.; Pfeil, S. H.; Hoffmann, A.; Streich, D.; Haenni, D.; Nettels, D.; Lipman, E. A.; Schuler, B. *Proc. Natl. Acad. Sci. U.S.A.* **2010**, *107*, 11793−11798.

(51) Pettersen, E. F.; Goddard, T. D.; Huang, C. C.; Couch, G. S.; Greenblatt, D. M.; Meng, E. C.; Ferrin, T. E. *J. Comput. Chem.* **2004**, *25*, 1605−1612.